

An experimental and theoretical study of gas tungsten arc welding of stainless steel plates with different sulfur concentrations

S. Mishra^a, T.J. Lienert^b, M.Q. Johnson^b, T. DebRoy^{c,*}

^a Department of Metallurgical Engineering and Materials Science, Indian Institute of Technology Bombay, Mumbai, India

^b Materials Science and Technology: Metallurgy Group, Los Alamos National Laboratory, Los Alamos, NM, USA

^c Department of Materials Science and Engineering, The Pennsylvania State University, University Park, PA, USA

Received 29 September 2007; received in revised form 18 December 2007; accepted 2 January 2008

Available online 6 March 2008

Abstract

During fusion welding, the presence of sulfur in steel often affects heat and fluid flow in the weld pool and its geometry. While the role of sulfur during welding of stainless steel plates with the same sulfur content is well understood, welding of stainless steel plates containing different concentrations of sulfur has not yet received proper attention. Here we report an experimental and modeling investigation of gas tungsten arc butt welding of stainless steel plates containing different sulfur concentrations. The main variables studied were sulfur concentrations in the two plates, welding current and welding speed. The results show significant shift of the fusion zone toward the low sulfur steel. The asymmetric fusion zone profile with respect to the original joint interface could be quantitatively explained through numerical modeling of heat transfer and fluid flow considering a bead shift observed experimentally.

© 2008 Published by Elsevier Ltd on behalf of Acta Materialia Inc.

Keywords: Stainless steel; Dissimilar sulfur concentrations; Welding

1. Introduction

When stainless steels (SSs) containing a surface active element such as sulfur are welded, the liquid metal flow pattern in the weld pool and the weld pool geometry may be significantly affected by its concentration. This phenomenon has been studied both experimentally and theoretically for the welding of two plates with similar sulfur concentrations [1–12]; for a given gas tungsten arc (GTA) welding procedure welds with low sulfur (<60 ppm S) typically have low depth/width aspect ratios, while welds with higher sulfur concentrations (>90 ppm) have higher aspect ratios, which typically approach or exceed 1.0.

A related but equally important need is to produce autogenous butt welds in SS plate or pipe where each half of the joint may have significantly different sulfur concen-

trations. Such situations are observed during autogenous welding of tube in pipe and in the nuclear waste management industry where stabilization, packaging and storage of plutonium-bearing materials involve welding of a low sulfur 316 SS container containing 0.003–0.006 wt.% sulfur with a higher sulfur 316 SS lid having more than 0.15 wt.% sulfur [13]. The welding of the container to its lid must be leak-tight and structurally sound [13–15]. Another example is the tungsten inert gas (TIG) welding of small diameter SS tubing for instrumentation systems in CANDU (Canadian Deuterium Uranium) nuclear reactors [12]. Experiments have shown that during welding of two SS plates with different sulfur contents, the point of maximum penetration shifts towards the plate with lower sulfur content [10,12]. In many cases, the weld bead shift is sometimes so severe that incomplete consumption of the joint can occur if procedures, tooling and the weld process are not tightly controlled. In order to ensure compliance with established fabrication standards it is necessary either to

* Corresponding author.

E-mail address: debroy@psu.edu (T. DebRoy).

control the materials being welded or to develop procedures that are insensitive to material composition [12].

Several studies aimed at rationalizing the problem have been reported. In an initial study, Heiple et al. [5] suggested an explanation for the shifting of the weld bead based on surface tension driven fluid flow model. They argued that the workpiece with lower sulfur content has a relatively higher surface tension than the one with higher sulfur content. They claimed the existence of a net surface tension gradient across the weld pool surface that resulted in fluid flow toward the low sulfur plate. However, in practice once the weld pool is formed, liquid metal in the weld pool circulates vigorously, mixing sulfur from the two plates. The actual surface tension gradients developed would then depend on the instantaneous sulfur distribution in the weld pool. Also, during a similar experiment, Rollin et al. [10] observed that the welding arc was displaced towards the low sulfur steel. They argued that the arc displacement should also be a contributing factor to the weld bead shift, along with the surface tension driven fluid flow [10]. A thorough quantitative understanding of the welding of two plates with different sulfur concentrations, which can take into account all the factors affecting weld bead shift, and predict the location, size and shape of the weld bead, is not available in the literature.

Here we report the result of an experimental and theoretical program of research aimed at understanding the GTA welding of three austenitic SSs containing 0.293, 0.024 and 0.003 wt.% sulfur. A well-tested three-dimensional numerical model of heat transfer, fluid flow and mass transfer is used to calculate the mixing and concentration field of sulfur in the weld pool, the temperature and velocity fields in the weld pool, and the resulting weld pool geometry. The effect of sulfur distribution in the weld pool on the convection pattern, and the shifting of the fusion zone towards the low sulfur side are identified as the two important factors contributing to the evolution of weld pool geometry. The calculated weld pool geometry considering sulfur distribution in the weld pool for a variety of welding conditions was compared with the corresponding experimental results.

2. Experimental procedure

Three austenitic SSs containing 0.003, 0.024 and 0.293 wt.% S, were used in the present study. The nominal compositions of the three steels are given in Table 1. Plates 50.8 mm wide, 254 mm long and 9.5 mm high were prepared for welding. Pairs of plates containing same and

different sulfur contents were welded using GTA welding. No preheat was used. Argon was used both as the welding and the shielding gas. The welding conditions are given in Table 2. The first six welds in the table correspond to the welding of plates having the same sulfur contents, while the rest of the cases are for the welding of plates with dissimilar sulfur concentrations. Two current levels and two welding speeds were employed in the experiments. Videos of selected welds were made using a video camera with no special filtering. After welding, conventional polishing and etching techniques were used to reveal the weld pool geometry, and to measure the weld pool width and penetration.

Electron probe microanalysis (EPMA) was used to measure concentration profiles of sulfur in the fusion zone for several cross-sections of the welds to check the accuracy of the calculated sulfur concentrations. Phosphorus concentration was also measured by EPMA to examine possible loss of elements present at low concentrations. The steels contained numerous manganese sulfide (MnS) precipitates, the size and density of which decreased with the decrease in the concentration of sulfur in steels. Therefore, if EPMA were done at a high spatial resolution, the results will show low concentration of sulfur in the matrix and a high concentration whenever a MnS precipitate is

Table 2
Welding conditions investigated

| Serial number | SS (left) | SS (right) | Current (A) | Voltage (V) | Welding speed (mm s ⁻¹) |
|---------------|-----------|------------|-------------|-------------|-------------------------------------|
| 1 | 304L | 304L | 101 | 9.6 | 1.7 |
| 2 | 304RL | 304RL | 100 | 9.6 | 1.7 |
| 3 | 304L | 304L | 150 | 9.9 | 1.7 |
| 4 | 303 | 303 | 150 | 10.5 | 1.7 |
| 5 | 304RL | 304RL | 100 | 10.0 | 3.4 |
| 6 | 303 | 303 | 101 | 9.9 | 3.4 |
| 7 | 304L | 303 | 150 | 10.5 | 1.7 |
| 8 | 304RL | 303 | 150 | 10.8 | 1.7 |
| 9 | 304L | 304RL | 150 | 10.5 | 1.7 |
| 10 | 304L | 303 | 150 | 10.8 | 3.4 |
| 11 | 304RL | 303 | 150 | 10.9 | 3.4 |
| 12 | 304L | 304RL | 150 | 10.7 | 3.4 |
| 13 | 304L | 303 | 100 | 9.8 | 1.7 |
| 14 | 304RL | 303 | 100 | 10.0 | 1.7 |
| 15 | 304L | 304RL | 100 | 9.9 | 1.7 |
| 16 | 304L | 303 | 100 | 10.2 | 3.4 |
| 17 | 304RL | 303 | 100 | 10.2 | 3.4 |
| 18 | 304L | 304RL | 100 | 10.0 | 3.4 |

Serial numbers 1–6 list the cases where the two welded specimens contained the same amount of sulfur. The remaining entries are for the cases where the two welded specimens contained different amounts of sulfur.

Table 1
Compositions of the three stainless steels (SS) used in the present study (compositions in wt.%)

| SS | C | P | S | Si | Mn | Cr | Ni | Mo | Ti | N | Cu | Co |
|-------|-------|-------|-------|-------|-------|--------|-------|-------|-------|-------|-------|-------|
| 304L | 0.022 | 0.028 | 0.003 | 0.303 | 1.811 | 18.537 | 8.453 | 0.296 | NA | 0.052 | 0.246 | NA |
| 304RL | 0.019 | 0.031 | 0.024 | 0.322 | 1.412 | 18.151 | 8.660 | 0.039 | 0.003 | 0.047 | 0.400 | 0.101 |
| 303 | 0.050 | 0.027 | 0.293 | 0.510 | 1.620 | 17.210 | 8.720 | NA | NA | NA | NA | NA |

encountered. In order to avoid this problem, the EPMA data was averaged over spot sizes of $50 \times 50 \mu\text{m}^2$ although EPMA can provide local concentrations at areas as small as $1 \mu\text{m}^2$.

3. Mathematical model

The following major assumptions are made in the model:

- (i) The molten metal is considered to be Newtonian and incompressible.
- (ii) The weld pool top surface is assumed to be flat.
- (iii) The density variation in the calculation domain is ignored except for the calculation of the buoyancy force following Boussinesq's approximation.

3.1. Governing equations

The transport phenomena inside the molten pool can be conveniently studied with respect to a coordinate system (x') that moves along the x -direction with the moving heat source by considering the following coordinate transformation:

$$x = x' - (-U)t, \quad (1)$$

where U is the welding speed and the torch moves along the negative x -direction, and x, y, z are coordinates in a frame moving with the welding torch. In the following discussion, the following notation will be followed for description of the conservation equations:

$$x_1 = x, \quad x_2 = y, \quad x_3 = z. \quad (2)$$

The momentum conservation equation in the moving coordinate system for the x -direction, with $i = 1, 2$ and 3 in index notation is given by

$$\rho \frac{\partial u_x}{\partial t} + \rho \frac{\partial u_i u_x}{\partial x_i} = -\frac{\partial p}{\partial x} + \frac{\partial}{\partial x_i} \left(\mu \frac{\partial u_x}{\partial x_i} \right) + \rho g \beta_T (T - T_r) + \rho g \beta_c (C - C_r) - \rho U \frac{\partial u_i}{\partial x_i} + S_x, \quad (3)$$

where u is the velocity, t is time, ρ is density, μ is viscosity, g is the gravitational acceleration, T_r is a reference temperature taken as the solidus temperature of the alloy, T_m , and C_r is the concentration of the solute at T_r . The terms β_T and β_c represent the thermal and solutal volumetric expansion coefficients, respectively. The source term S_x considers frictional resistance to flow experienced by the liquid metal in the two-phase solid–liquid region similar to flow in a porous medium. This resistance is calculated using Darcy's model and the Carman–Kozeny relationship [16–18]. The source term also includes the Lorentz force as a consequence of the electric current used in the welding [19]. Combining these two effects, the source term can be represented as

$$S_x = -\frac{K_m(1-f_l)^2}{f_l^3 + b} u_x + (J \times B)_x, \quad (4)$$

where f_l is the liquid fraction given as: $f_l = \Delta H/L$, ΔH is the latent heat content of a control volume, L is the latent heat of fusion, J is the current density and B is the magnetic field intensity. In Eq. (4), K_m is a large number [16] and b is a small number to avoid division by zero. The above formulation ensures that the velocity becomes zero in the solid region and increases continuously into the liquid region. The details of the formulation of the above term have been reported by Brent et al. [18]. The calculation of the Lorentz force term is presented in the literature [19], and is not repeated here. Momentum balance equations similar to Eq. (3) were also solved for the y and z directions.

The pressure field was obtained by solving the following continuity equation simultaneously with the momentum equations [16,17]:

$$\frac{\partial u_i}{\partial x_i} = 0. \quad (5)$$

The total enthalpy, H , is represented by a sum of sensible heat, h , and latent heat content, ΔH , i.e. $H = h + \Delta H$, where $h = \int C_p dT$, C_p is the specific heat, T is the temperature, $\Delta H = f_l L$, L is the latent heat of fusion, and the liquid fraction, f_l , is assumed to vary linearly with temperature in the mushy zone [16,17]:

$$f_l = \begin{cases} 1 & T > T_1, \\ \frac{T-T_s}{T_1-T_s} & T_s \leq T \leq T_1, \\ 0 & T < T_s, \end{cases} \quad (6)$$

where T_1 and T_s are the liquidus and the solidus temperature, respectively. The thermal energy transport in the workpiece can be expressed by the following modified energy equation [16,17]:

$$\rho \frac{\partial h}{\partial t} + \rho \frac{\partial (u_i h)}{\partial x_i} = \frac{\partial}{\partial x_i} \left(\frac{k}{C_p} \frac{\partial h}{\partial x_i} \right) - \rho \frac{\partial \Delta H}{\partial t} - \rho \frac{\partial (u_i \Delta H)}{\partial x_i} - \rho U \frac{\partial h}{\partial x_i} - \rho U \frac{\partial \Delta H}{\partial x_i}, \quad (7)$$

where k is the effective thermal conductivity. In the liquid region, the thermal conductivity in Eq. (7) is taken as the effective thermal conductivity, which is a property of the specific welding system and not a physical property of the liquid metal. Typical values of effective thermal conductivity are much higher than that of the thermal conductivity of the liquid. The higher value is important because it allows accurate modeling of the high rates of transport of heat in systems with strong fluctuating velocities that are inevitable in small weld pools with very strong convection currents [20,21]. The species conservation equation is given by

$$\frac{\partial (\rho C)}{\partial t} + \frac{\partial (\rho u_i C)}{\partial x_i} = \frac{\partial}{\partial x_i} \left(\rho D \frac{\partial C}{\partial x_i} \right) - \rho U \frac{\partial C}{\partial x_i}, \quad (8)$$

where C is the solute concentration and D is the effective mass diffusivity of the solute. The incorporation of solute conservation equation in the numerical model allows the calculation of sulfur concentration distribution in the weld

and provides information about its role on weld pool development.

3.2. Boundary conditions

The velocity boundary conditions are given as [16,17]:

$$\begin{aligned} \mu \frac{\partial u}{\partial z} &= f_1 \left(\frac{\partial \gamma}{\partial T} \frac{\partial T}{\partial x} + \frac{\partial \gamma}{\partial C} \frac{\partial C}{\partial x} \right), \\ \mu \frac{\partial v}{\partial z} &= f_1 \left(\frac{\partial \gamma}{\partial T} \frac{\partial T}{\partial y} + \frac{\partial \gamma}{\partial C} \frac{\partial C}{\partial y} \right), \\ w &= 0, \end{aligned} \quad (9)$$

where u , v and w are the velocity components along the x , y and z directions, respectively, $d\gamma/dC$ is the concentration coefficient of surface tension and $d\gamma/dT$ is the temperature coefficient of surface tension. The $\partial\gamma/\partial C$ term has been incorporated in Eq. (9) in the present study because the distribution of solute in the weld pool is not necessarily uniform and therefore $\partial C/\partial x$ and $\partial C/\partial y$ have finite values. As shown in Eq. (9), the u and v velocities at the surface are determined from the Marangoni effect [16,17]. The w velocity is zero since there is no flow of liquid metal perpendicular to the weld pool top surface. The heat flux at the top surface is given by [16,17]

$$k \frac{\partial T}{\partial z} = \frac{dQ\eta}{\pi r_b^2} \exp\left(-\frac{d(x^2 + y^2)}{r_b^2}\right) - \sigma\epsilon(T^4 - T_a^4) - h_c(T - T_a), \quad (10)$$

where r_b is the arc radius of a circular region within which the arc power is focused, d is the dimensionless arc power distribution factor, which determines the nature of distribution of the power density of the arc, Q is the total arc power, η is the arc efficiency, σ is the Stefan–Boltzmann constant, h_c is the heat transfer coefficient, and T_a is the ambient temperature. The first term on the right-hand side of Eq. (10) is the heat input from the heat source, defined by a Gaussian heat distribution. The arc power distribution factor, d , determines the nature of the Gaussian heat distribution pattern. The distribution is rather diffuse for low values of d such as 0.5 and more focused for higher values of d such as 3.0. The second and third terms represent the heat loss by radiation and convection, respectively. The lateral position of the heat source was determined from the experimental results for each weld. Details of the procedure are presented subsequently. At all other surfaces, temperatures are taken as ambient temperature and the velocities are set to zero.

3.3. The effect of sulfur on weld pool convection

The temperature coefficient of surface tension ($\partial\gamma/\partial T$) for pure metals is negative. The presence of sulfur in the weld pool can make the value of $\partial\gamma/\partial T$ positive [1–5]. For liquid metals with a positive value of $\partial\gamma/\partial T$, the direction of the Marangoni stress and the resulting flow pattern

may affect the weld pool geometry. Surface tension of a binary Fe–S alloy is given as a function of both temperature and activity of sulfur as [2]:

$$\gamma = \gamma_m - A[T - T_m] - RT\Gamma_s \ln[1 + Ka_s], \quad (11)$$

$$K = k_1 \exp\left(-\frac{\Delta H^\circ}{RT}\right), \quad (12)$$

where γ_m is the surface tension of the pure metal at melting point, T_m is the melting point of the material, a_s is the activity of sulfur, A is negative of $\partial\gamma/\partial T$ for pure metal, Γ_s is the surface excess at saturation, k_1 is the entropy factor, and ΔH° is the standard enthalpy of adsorption. The validity of Eq. (11) for application in SS has been demonstrated in Ref. [22]. By differentiating Eq. (11) with respect to temperature, the expression for $\partial\gamma/\partial T$ as a function of both temperature and sulfur concentration can be obtained as [2]:

$$\frac{\partial\gamma}{\partial T} = -A - R\Gamma_s \ln[1 + KC] - \frac{KC}{1 + KC} \Gamma_s (\Delta H^\circ - \Delta \bar{H}_s^m), \quad (13)$$

Table 3
Data used in the calculations

| Problem data/physical property | Value |
|--|------------------------|
| Liquidus temperature, T_l (K) | 1785.0 |
| Solidus temperature, T_s (K) | 1745.0 |
| Density of metal, ρ (kg m^{-3}) | 7200.0 |
| Thermal conductivity of solid, k_s ($\text{J m}^{-1} \text{s}^{-1} \text{K}^{-1}$) | 25.08 |
| Specific heat of solid, C_{ps} ($\text{J kg}^{-1} \text{K}^{-1}$) | 702.24 |
| Specific heat of liquid, C_{pl} ($\text{J kg}^{-1} \text{K}^{-1}$) | 806.74 |
| Temperature coefficient of surface tension, $d\gamma/dT$ ($\text{N m}^{-1} \text{K}^{-1}$) | -0.47×10^{-3} |
| Coefficient of thermal expansion, β (K^{-1}) | 1.50×10^{-6} |
| Viscosity of liquid, μ_l ($\text{kg m}^{-1} \text{s}^{-1}$) | 6.70×10^{-3} |
| Surface excess of sulfur at saturation, Γ_s (mol m^{-2}) | 1.30×10^{-3} |
| Enthalpy of adsorption for sulfur, ΔH° ($\text{J kg}^{-1} \text{mol}^{-1}$) | -1.66×10^6 |
| Entropy factor, k_1 | 3.18×10^{-3} |

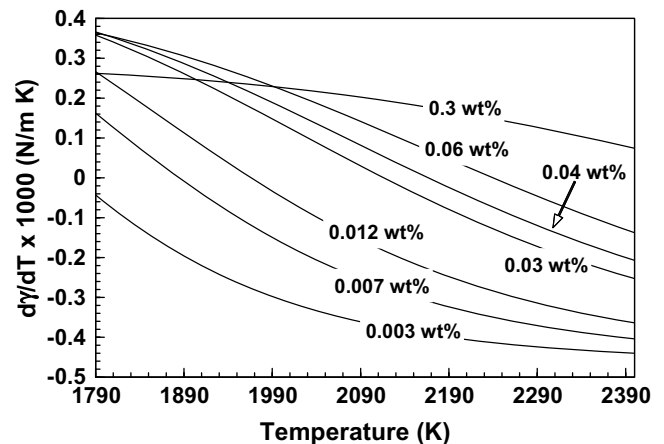


Fig. 1. Computed temperature coefficient of surface tension, $d\gamma/dT$, as a function of temperature for stainless steel specimens containing 0.003, 0.007, 0.012, 0.03, 0.04, 0.06 and 0.3 wt.% sulfur.

where $\Delta\bar{H}_s^m$ is the partial molar enthalpy of mixing of sulfur in the solution. For a dilute solution of sulfur in iron, $\Delta\bar{H}_s^m$ is taken as zero [2]. Using Eq. (13) and the data presented in Table 3 $\partial\gamma/\partial T$ is plotted as a function of temperature for different sulfur concentrations in Fig. 1. It can be seen that for low sulfur concentrations such as 0.003 wt.%, $\partial\gamma/\partial T$ is negative over the entire temperature range. Negative $\partial\gamma/\partial T$ causes the liquid to move from the center to the periphery on the weld pool surface leading to a wide and shallow weld pool. On the other hand, for very high sulfur concentrations such as 0.3 wt.%, $\partial\gamma/\partial T$ is positive over the entire temperature range. Positive $\partial\gamma/\partial T$ causes the liquid to move from the periphery to the center of the weld pool surface leading to a narrow and deep weld pool. When the two plates being welded have different sulfur concentrations, the value of $\partial\gamma/\partial C$ in Eq. (9) needs to be calculated by differentiating Eq. (11) with respect to sulfur concentration:

$$\frac{\partial\gamma}{\partial C} = -\frac{RT\Gamma_s K}{1 + KC} \quad (14)$$

The thermophysical data used in the calculations are given in Table 3. The same set of data was used for all the three SSs listed in Table 1, because the difference in the values of physical properties of the three steels was less than 2% [23].

Because of the high temperatures involved during fusion welding, vaporization of alloying elements takes place from the top surface. Possible loss of sulfur is considered in the model by applying a mass loss boundary condition at the top surface. The procedure used in the calculation of sulfur loss is described in Appendix A. However, the loss of sulfur from the top surface was found to be insignificant for the conditions of the present study.

As discussed later in Section 4, simulations made assuming surface tension driven fluid flow without introducing a shift in the position of the heat source in the model did not provide accurate results. Hence, a shift in the position of the arc was incorporated into the model that was based on experimental results and that took account of weld current, travel speed and differences in sulfur content between the two workpieces.

4. Results and discussion

4.1. Weld pool geometry for two plates with same sulfur concentration

The effect of sulfur in the welding of steels from the same heat has been well studied [1–12]. Therefore, as a first step, the numerical transport phenomena based model developed in the present study was validated by applying it to GTA welding of SS plates having the same sulfur contents.

The effect of sulfur on weld pool geometry can be observed by comparing Fig. 2a and b. These two figures show the experimental and the calculated weld pool geometries for SS welds containing 0.003 and 0.024 wt.% sulfur, respectively, welded under the same set of welding param-

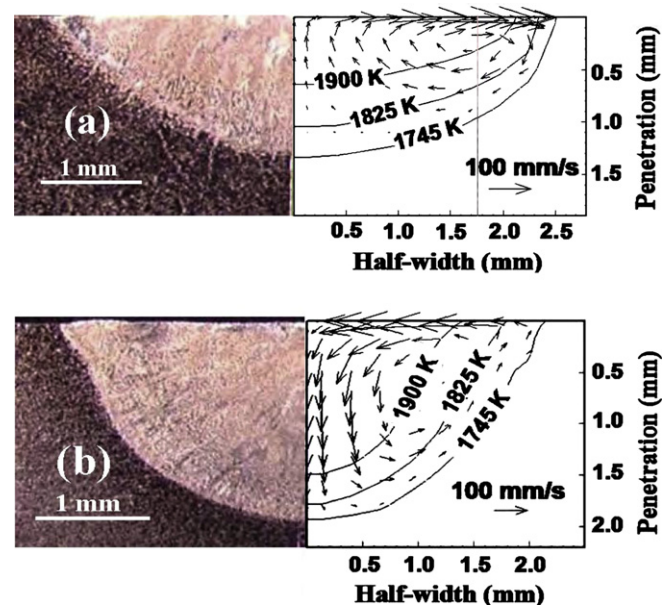


Fig. 2. Experimental and calculated weld pool geometries, (a) and (b) correspond to welds 1 and 2 of Table 4. The solidus temperature of stainless steel marks the weld pool boundary.

eters. It can be seen that the weld containing 0.024 wt.% sulfur has a much deeper penetration than that containing 0.003 wt.% sulfur.

The difference in the pool shape in the two cases can be attributed to the well-known difference in fluid flow pattern in the weld pool. The direction of liquid flow is governed by the sign of $\partial\gamma/\partial T$. It can be seen from Fig. 1 that for 0.003 wt.% sulfur, $\partial\gamma/\partial T$ is negative for the entire temperature range of the plot. The negative value of $\partial\gamma/\partial T$ results in an outward flow and consequently a relatively shallow weld pool is formed in Fig. 2a. In Fig. 2b, the specimen contains 0.024 wt.% sulfur, and Fig. 1 shows that for such high sulfur contents, $\partial\gamma/\partial T$ is positive up to about 2100 K. Positive $\partial\gamma/\partial T$ causes the convection pattern to be radially inwards resulting in a relatively deep weld pool. When the sulfur concentration is high, the hot liquid metal under the arc moves downwards in the middle of the weld pool and enhances the weld pool depth as shown in Fig. 2b. In contrast, in low sulfur containing weld pool, the hot liquid metal in the middle of the weld pool is transported from the middle to the edge of the weld pool as shown in Fig. 2a. The direction of recirculation in a low sulfur weld pool is opposite to that in a high sulfur weld pool and the opposite recirculation pattern causes a significant difference in the geometry of the weld pool because convective transport of heat is the main mechanism of heat transfer in the weld pool as will be established below. Similar trends in fluid flow and weld pool shapes were found with welds 3 and 4 of Table 4. For welds 5 and 6 of Table 4, both concentrations of sulfur result in similar inward liquid flow pattern over the range of temperature prevalent over the weld pool surface. Good agreement between the calculated and measured weld pool geometries for welds 1–6 in Table

Table 4
Welding variables and experimentally measured weld pool penetration and width

| Weld number | Current (A) | Voltage (V) | Welding speed (mm s ⁻¹) | Sulfur (wt.%) | Weld pool depth (mm) | | Weld pool width (mm) | |
|-------------|-------------|-------------|-------------------------------------|---------------|----------------------|------|----------------------|------|
| | | | | | Exp | Cal | Exp | Cal |
| 1 | 101 | 9.6 | 1.7 | 0.003 | 1.37 | 1.36 | 4.83 | 4.93 |
| 2 | 100 | 9.6 | 1.7 | 0.024 | 1.94 | 1.97 | 4.37 | 4.41 |
| 3 | 150 | 9.9 | 1.7 | 0.003 | 2.18 | 2.02 | 6.80 | 6.93 |
| 4 | 150 | 10.5 | 1.7 | 0.293 | 3.12 | 3.09 | 5.91 | 6.07 |
| 5 | 100 | 10.0 | 3.4 | 0.024 | 1.22 | 1.27 | 4.15 | 4.13 |
| 6 | 101 | 9.9 | 3.4 | 0.293 | 1.39 | 1.41 | 4.05 | 4.10 |

'Exp' stands for experimental results while 'Cal' stands for calculated results.

4 indicates that the role of sulfur on the weld pool geometry is predicted reasonably well by the numerical transport phenomena based model used in the investigation.

The relative importance of convection and conduction in the overall transport of heat in the weld pool can be assessed from the value of the Peclet number, Pe_h , which is given by:

$$Pe_h = \frac{u\rho C_p L}{k}, \quad (15)$$

where u is the velocity, ρ is the density, C_p is the specific heat at constant pressure, L is the characteristic length taken as the half-width of the weld pool, and k is the thermal conductivity of the melt. When Pe_h is large, heat is transported mainly by convection. The data used for the calculation of Pe_h and the computed values for the six welds listed in Table 4 are presented in Table 5. The values of the Peclet number for all the six cases are much higher than one. The high values of Peclet number indicate that convection is the dominant mechanism of heat transfer in the weld pool. As a result, the weld pool geometry is largely determined by the direction of the liquid flow in the weld pool.

4.2. Welding of two plates with different sulfur concentrations

4.2.1. The common features of welds

In order to understand the key features of the welding of steels with dissimilar sulfur contents, let us consider Fig. 3 that shows the cross-section of a weld where a 304L SS plate (left plate) with 0.003 wt.% sulfur is welded to a 303 SS plate (right plate) with 0.293 wt.% sulfur. The original interface of the two plates is denoted by the vertical white line next to location 'A' in Fig. 3. The following four key features can be observed:

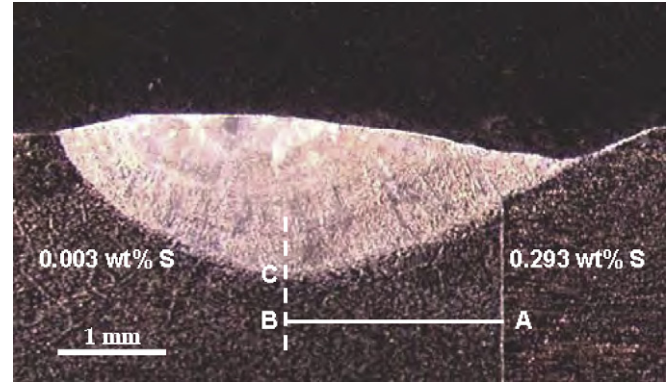


Fig. 3. Weld pool geometry when welding a stainless steel plate having low sulfur content (0.003 wt.%) with a plate having very high sulfur content (0.293 wt.%). The white vertical line at location 'A' indicates the joint of the two plates. Location 'C' indicates the point of maximum penetration. Line 'AB' denotes the shift of the point of maximum penetration from the joint of the two plates. The length of line 'AB' is called the center line shift (CLS). Welding conditions: 100 A, 9.8 V, and 1.7 mm s⁻¹ welding speed.

- The weld bead is shifted towards the plate containing lower sulfur with less melting on the high sulfur side. The cross-section in Fig. 3 shows a weld with a missed joint.
- The point of maximum penetration, C, is shifted by a distance AB from the original joint of the two plates. The length AB will be referred as the center line shift (CLS) [12].
- Videos taken during our experiments showed an asymmetry of the arc for the dissimilar sulfur welds with flaring out of the periphery of the arc just above the workpiece surface. An example of the flaring of the arc is given in Fig. 4. However, no shifting or rotating of the central arc column was detected.

Table 5
The values of Peclet numbers (Pe_h) for heat transfer for the six cases listed in Table 4 and shown in Fig. 2

| Weld number | Velocity, u (m s ⁻¹) | Density, ρ (kg m ⁻³) | Specific heat, C_p (J kg ⁻¹ K ⁻¹) | Length, L (m) | Thermal conductivity, k (W m ⁻¹ K ⁻¹) | Peclet number, Pe_h |
|-------------|------------------------------------|---------------------------------------|--|-----------------|--|-----------------------|
| 1 | 0.235 | 7200 | 807.1 | 0.0024 | 125.5 | 26 |
| 2 | 0.256 | 7200 | 807.1 | 0.0022 | 125.5 | 26 |
| 3 | 0.384 | 7200 | 807.1 | 0.0034 | 125.5 | 62 |
| 4 | 0.279 | 7200 | 807.1 | 0.0030 | 125.5 | 40 |
| 5 | 0.208 | 7200 | 807.1 | 0.0020 | 125.5 | 20 |
| 6 | 0.263 | 7200 | 807.1 | 0.0020 | 125.5 | 26 |

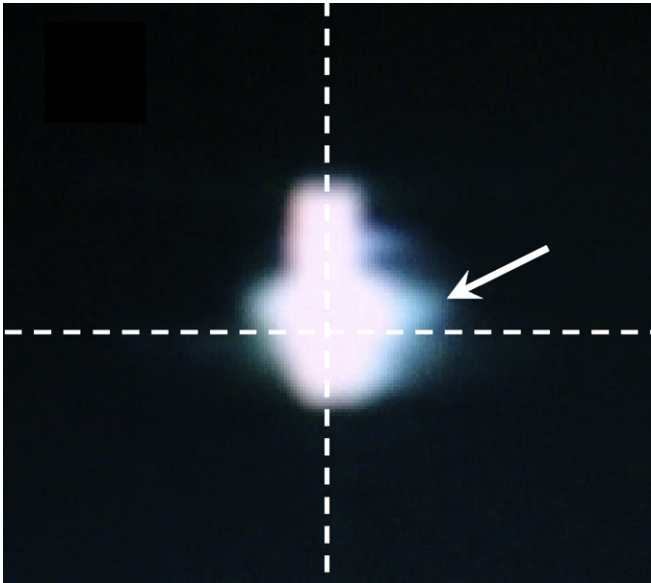


Fig. 4. The still photograph extracted from the video shows arc asymmetry during a weld between the 304L (low sulfur, right) and 303 (high sulfur, left) alloys. Note the flaring out of the arc towards the low sulfur plate just above the workpiece surface, as indicated by the arrow. The vertical dotted line gives the original interface of the two plates, while the horizontal dashed line indicates the approximate position of the workpiece surface. Bright features below the horizontal dashed line are due to reflections from the weld pool and are not pertinent.

Similar observations have been reported for GTA welds made between plates of 316 SS with different sulfur contents by other investigators [10]. Moreover, Bennett and Mills [24] found differences in the shape of the arc for GTA welds made between workpieces from the same heats of 21-6-9 SSs as a function of the weld depth-to-width ratio (D/W) (and presumably the content of surface active elements in each heat). Using photographs of the arc and spectroscopy, they showed that the arcs for low D/W welds (presumably with low surface active element content) flared out near the workpiece surface relative to high D/W welds, and that the flared region corresponded to manganese emission.

- (d) An undercut can be seen on the high sulfur side, while an over-fill can be seen on the low sulfur side, indicating a net movement of mass from the high sulfur side to the low sulfur side. Comparison of all the experiments shows that the undercut is more severe in cases involving 303 SS, which has very high sulfur content.

The occurrence of the weld bead shift has been demonstrated in the present study by conducting the following welding experiment with low and high sulfur plates. One set of plates was placed so that the steel containing 0.024 wt.% sulfur was on the right-hand side of the welding torch and a plate with 0.003 wt.% sulfur on the left-hand side. A second set of plates were placed in the reverse configuration, i.e. the low sulfur (0.003 wt.%) plate was placed on the right and the high sulfur (0.024 wt.%) plate on the left side of the welding torch. The weld started on the first set and continued onto the second set as shown in Fig. 5. The resulting shift of the weld bead can be observed at the crossover from the first to the second set of plates.

4.2.2. Role of sulfur and heat input on the extent of bead shift

An important question is how far does the bead shift from the original interface of the two plates? The shift is quantified by the CLS, which is given by the length of line AB in Fig. 3. Table 6 lists the CLS values determined from the weld cross-sections. It can be seen from the table that the energy input is an important factor in affecting CLS. For example, for the same SS combination, the CLS for weld 1 having higher energy input is higher than that for weld 10 with lower energy input. Furthermore, a comparison of welds 1–3 in Table 6 shows that for approximately the same energy input, the difference in the sulfur content of the two plates also affects CLS. It is observed from the table that CLS does not depend linearly on the two factors. A three parameter optimization was conducted to get the values of a, b and c in the following equation from the experimental data in Table 6:

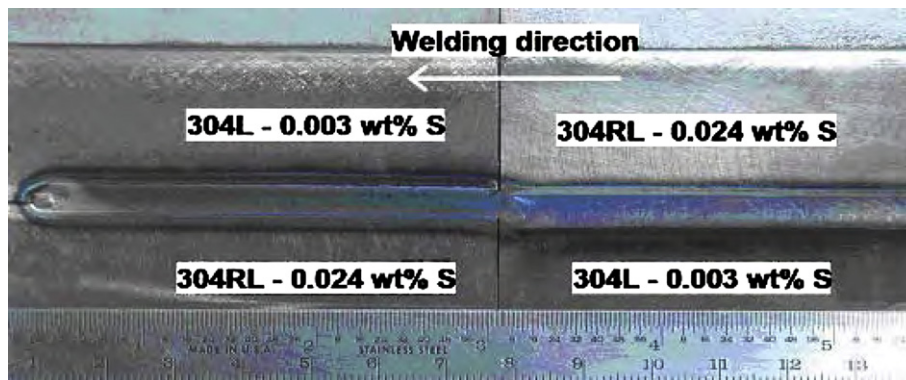


Fig. 5. An experiment to demonstrate the shifting of the arc towards the low sulfur side. At the start of welding, a 304RL steel containing 0.024 wt.% sulfur is placed on the right hand side of the torch and a 304L plate with 0.003 wt.% sulfur is placed on the left hand side. After half way along the length of the weld, the plates were switched. The resulting shift of the weld bead can be observed in the figure.

Table 6
The center line shift (CLS) of all the experimental results for welding of plates with different sulfur contents

| Weld number | SS (left) | SS (right) | $ C_L - C_R $ (wt.% S) | Current (A) | Voltage (V) | Welding speed (mm s^{-1}) | Energy input (J mm^{-1}) | CLS (mm) |
|-------------|-----------|------------|------------------------|-------------|-------------|--------------------------------------|-------------------------------------|----------|
| 1 | 304L | 303 | 0.293 | 150 | 10.5 | 1.7 | 926.47 | 2.44 |
| 2 | 304RL | 303 | 0.270 | 150 | 10.8 | 1.7 | 952.94 | 2.68 |
| 3 | 304L | 304RL | 0.023 | 150 | 10.5 | 1.7 | 926.47 | 1.77 |
| 4 | 304L | 303 | 0.293 | 150 | 10.8 | 3.4 | 476.47 | 2.16 |
| 5 | 304RL | 303 | 0.270 | 150 | 10.9 | 3.4 | 480.88 | 2.22 |
| 6 | 304L | 304RL | 0.023 | 150 | 10.7 | 3.4 | 472.06 | 1.32 |
| 7 | 304L | 303 | 0.293 | 100 | 9.8 | 1.7 | 576.47 | 1.88 |
| 8 | 304RL | 303 | 0.270 | 100 | 10.0 | 1.7 | 588.24 | 1.38 |
| 9 | 304L | 304RL | 0.023 | 100 | 9.9 | 1.7 | 582.35 | 0.80 |
| 10 | 304L | 303 | 0.293 | 100 | 10.2 | 3.4 | 300.00 | 1.51 |
| 11 | 304RL | 303 | 0.270 | 100 | 10.2 | 3.4 | 300.00 | 1.52 |
| 12 | 304L | 304RL | 0.023 | 100 | 10.0 | 3.4 | 294.12 | 0.80 |

SS stands for stainless steel. C_L is the sulfur concentration in wt.% in the left piece while C_R is the sulfur concentration in wt.% in the right piece. The value of heat input (J mm^{-1}) is given by (current \times voltage/welding speed).

$$CLS = a \times |C_L - C_R|^b \times \left(\frac{I \times V}{U}\right)^c, \quad (16)$$

where CLS is the center line shift in mm, C_L is the sulfur content of the left plate in wt.%, C_R is the sulfur content of the right plate in wt.%, I is the current in A, V is voltage in V and U is the welding speed in mm s^{-1} . The optimized values were $a = 0.19$, $b = 0.24$ and $c = 0.42$. A plot of CLS vs. the right-hand side of Eq. (16) is shown in Fig. 6. The symbols represent the experimental data and the line represents a linear fit to the experimental data. The linear fit passes through the origin so that CLS is zero when the two plates have the same sulfur content. The empirical relation in Eq. (16) takes into account the effect of both the heat input and the difference in sulfur contents of the two plates, and can be readily used to approximately estimate the location of the arc during welding.

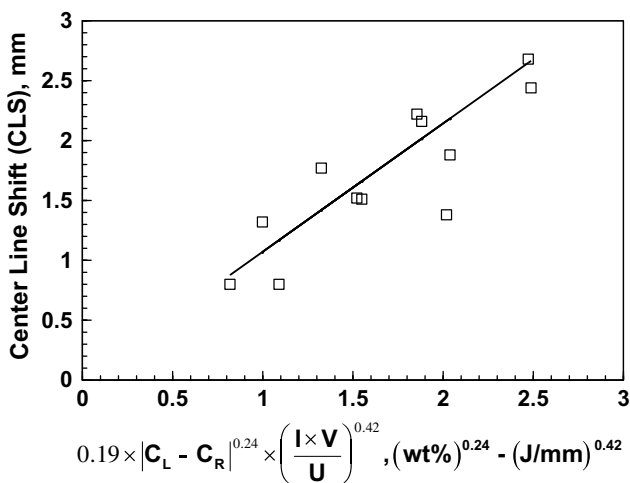


Fig. 6. Relation between the center line shift (CLS) and the two factors affecting it, i.e., absolute value of difference in sulfur content of the two plates and the heat input per unit length. The symbols represent the experimentally measured data while the line represents the linear fit to the experimental data. The symbol C_L is the sulfur content of the left plate (wt.%), C_R is the sulfur content of the right plate (wt.%), I is current (A), V is voltage (V) and U is the welding speed (mm s^{-1}).

Tinkler et al. [12] also explored the link between sulfur content and CLS. They welded several SS tubes containing between 15 ppm (1 ppm = 10^{-4} wt.%) and 140 ppm sulfur

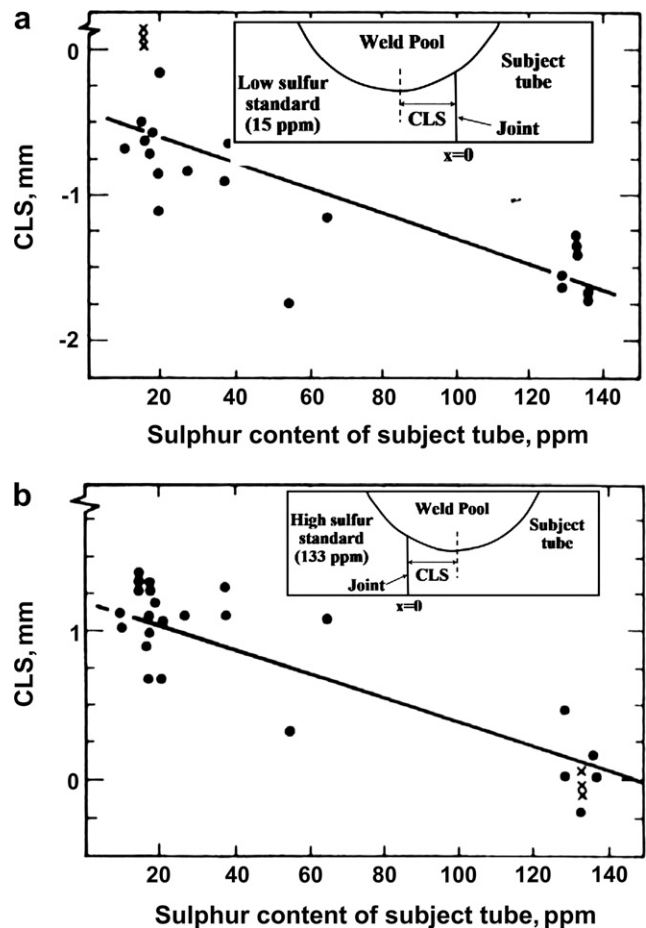


Fig. 7. Variation of center line shift (CLS) with sulfur content when subject tubes were welded to: (a) low sulfur standard, i.e., 15 ppm (0.0015 wt.%) sulfur, (b) high sulfur standard, i.e., 133 ppm (0.0133 wt.%) sulfur [12]. The solid circles represent the results for cases where the two tubes had different sulfur contents. The crosses represent the cases where the two tubes had the same sulfur content. Welding conditions: start current: 35 A, finish current: 26 A, fixture rotation speed: 4.6 rpm, and outer diameter of tubing: 9.5 mm. Unit conversion: 1 ppm = 10^{-4} wt.%.

with standard SS tubes containing 15 ppm or 133 ppm sulfur [12]. Their results for the variation of CLS on welding various SS tubes to low sulfur (15 ppm) standard and high sulfur (133 ppm) standard are shown in Fig. 7a and b, respectively [12]. All the experiments were performed using the same heat input. In their experiments, the standard tube was kept on the left-hand side and the subject tube was kept on the right-hand side [12]. The $x = 0$ location corresponded to the joint of the two plates. Since the weld pool shifts towards the low sulfur side, the CLS values were negative for all the cases involving the low sulfur standard, as shown in Fig. 7a, and positive for majority of cases involving the high sulfur standard as shown in Fig. 7b. In these figures the solid circles represent the results for cases where the two tubes had different sulfur contents, while the crosses represent the cases where the two tubes had the same sulfur content. When the two tubes had the same sulfur content, the CLS was almost zero. The data points in both Fig. 7a and b were mostly clustered at the two extremes of the sulfur content range considered in the experiments. Furthermore, Tinkler et al. [12] did not consider the effect of heat input, which is an important factor influencing CLS, as can be seen from Table 6.

Heiple et al. [5] suggested that the undercut resulted from the surface tension driven fluid flow because the plate with lower sulfur content has a relatively higher surface tension than the one with higher sulfur content. They argued that the presence of a net surface tension gradient across the weld pool leads to fluid flow toward the plate with lower sulfur content. However, they did not consider mixing of sulfur in the weld pool or examine the role of fluid flow in the fusion zone shift experimentally or theoretically [5]. Heat transfer, fluid flow and the transport of sulfur must be considered together with the arc asymmetry to understand the occurrence of undercut.

4.2.3. Toward understanding the bead shift

In order to understand the observed bead shift, it is useful to discuss the following underlying issues:

1. The electrode tip remains vertically above the interface between the two plates containing different concentrations of sulfur at all times during welding. At the initiation of welding, the arc extends from the tip of the electrode to the cathode spot at the interface of the two plates. Melting of both plates commences immediately after the arc is struck.
2. As the melting begins, alloying elements start to vaporize from the surface of both plates. Two main factors that govern the local rates of vaporization of alloying elements are the local temperature and the activities of each alloying elements that depend mainly on local alloy composition and temperature. At the initiation of melting, it is fair to assume that the temperatures on both sides of the original interface are not significantly different. However, the activities of manganese in the first liquid that forms from the high sulfur steel would be significantly lower than that in the low sulfur steel. This is because in the high sulfur steel, manganese is present mainly as MnS precipitates and, as a result, relatively less manganese is present in solution in the alloy. In contrast, in the low sulfur steel, very little MnS is present, and practically all the manganese is present as an alloying element in the alloy. As a result, in the first liquid to form, the manganese activity is higher in the low sulfur steel than that in the high sulfur steel. Although the temperatures are roughly symmetrical on both sides of the original joint interface, this difference in the activity leads to a higher evaporation rate of manganese for the low sulfur steel compared to the high sulfur steel.
3. At the initiation of melting, the higher rates of evaporation of manganese over the low sulfur steel leads to higher concentration of easily ionizable manganese vapor over this region. The electrical conductivity of the arc over the low sulfur steel increases significantly because of the presence of manganese vapor [25,26]. The higher electrical conductivity of the arc over the low sulfur side, in turn, provides a preferential high conducting path for the arc. As a result, the arc flares out toward the lower sulfur containing plate. It is thought that the flaring out of the arc involves movement of the cathode spot on the surface of the low sulfur plate away from the high sulfur plate, heating this plate preferentially. As a result, the temperatures in the low sulfur plate becomes higher than that in the high sulfur plate, and the vaporization rate of all alloying elements increase over this plate; higher partial pressures of metal vapors over this region progressively broadens the arc further locally. Once the low sulfur plate melts in preference to the high sulfur plate and most metal vapors are above the low sulfur plate, preferential melting of the low sulfur plate continues during the entire welding process.
4. During heating of dissimilar alloys, the thermoelectric effect (Seebeck) and the resulting current distribution can lead to an electromagnetic force field. Depending on the magnitude of the forces, it may deflect electrons in the arc and potentially contribute to the arc asymmetry. The Seebeck electromagnetic force field depends on the thermoelectric (Seebeck) potentials for the high and low sulfur alloys at various temperatures. These data are not available in the literature. However, it is possible to calculate, through dimensional analysis, the values of Seebeck potentials needed for this effect to be important. If these computed potentials are of the same order of magnitude as those reported for other alloy pairs in the literature, it could be argued that the Seebeck effect is a contributing factor in the arc asymmetry. The Seebeck magnetic Reynolds number, Re_S , which is the ratio of Seebeck electromagnetic force to viscous force is given by $Re_S = \rho \mu_0 \mu_r I^2 / (4\pi^2 \mu^2)$, where ρ is the density of liquid metal (7000 kg m^{-3}), μ_0 is the permeability of free space ($4\pi \times 10^{-7} \text{ N/A}^2$), μ_r is the relative permeability (1.0), I is the Seebeck current (unknown), and μ is the viscosity of

the liquid metal ($5 \times 10^{-3} \text{ kg m}^{-1} \text{ s}^{-1}$). For the Seebeck force to be of the same order of magnitude as the surface tension force, the Seebeck magnetic Reynolds number should be of the same order of magnitude as the surface tension Reynolds number for a typical welding condition which is the ratio of surface tension force to viscous force (10^4). For a value of $Re_S = 10^4$, the computed value of current, I , is 33.5 A. The corresponding Seebeck coefficient, s , is given by $I/(\sigma\Delta TL)$ where σ is the electrical conductivity ($1.5 \times 10^6 \text{ mho m}^{-1}$), ΔT is the temperature difference (1000 K), and L is the length scale (10^{-3} m). For the values of each parameter given within brackets, the computed value of the Seebeck coefficient is $2.2 \times 10^{-5} \text{ V K}^{-1}$. This value is of the same order of magnitude but somewhat higher than the values reported for most alloy combinations [27]. The order of magnitude calculations show that a possible contribution by the Seebeck electromagnetic force cannot be ruled out.

5. The shifting of the weld bead to the low sulfur side is consistent with the flaring of the arc toward the low sulfur side.
6. The maximum extent of the arc flare can be determined by assuming that the deepest location of the weld pool lies directly below the cathode spot. In the range of variables reported in this paper, the maximum extent of the arc asymmetry is determined by the heat input and the difference in the sulfur concentrations in the two plates as discussed previously in the paper.

4.2.4. Heat transfer, fluid flow and mass transfer

The numerical transport phenomena based model developed in the present study was used to calculate the evolution of weld pool geometry for all the cases listed in Table 6. As mentioned earlier, simulations made assuming that the arc heat source was centered on the jointline and incorporating surface tension driven fluid flow did not match experimental results found in metallographic cross-sections. Results of these simulations are not shown for the sake of brevity. To achieve better correspondence with the experimental results, the model assumed that the arc was shifted by a distance equal to the experimentally measured value of CLS in each case. The calculated weld pool geometries for three cases listed in Table 6 are compared with the corresponding experimental micrographs in Figs. 8–10. In each figure, part (a) shows the experimental weld pool geometry and part (b) shows the computed temperature contours in Kelvin and the liquid velocity vectors by the size of the arrows. Part (c) shows the computed contours of sulfur concentration in wt.% in the weld pool.

Since fluid flow pattern and the temperature fields in the weld pool are affected by the sulfur concentration, these are examined first. Fig. 8c shows the computed sulfur concentration field for the welding of two plates containing 0.293 and 0.003 wt.% S. An important aspect of sulfur distribution in the weld pool is observed from this figure. On the surface of the weld pool, significant concen-

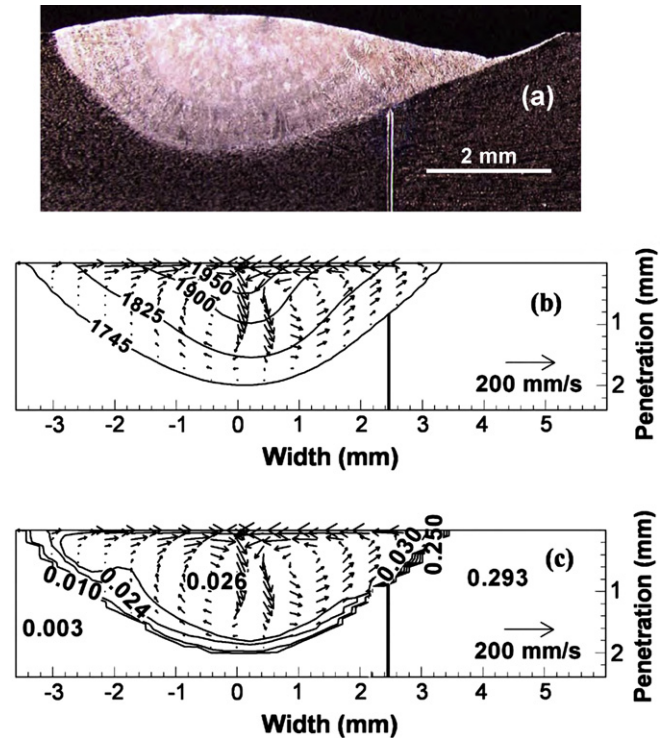


Fig. 8. Results for weld 1 in Table 6. (a) Experimental weld pool geometry. The vertical line shows the original interface of the two plates. (b) Calculated temperature and velocity fields in the weld pool. The contours represent the temperatures in degree Kelvin and the vectors represent the liquid velocity. (c) The contours represent calculated sulfur concentrations in wt.%. The sulfur concentration on the top surface and the bulk of the weld pool was about 0.026 wt.%. Welding conditions: 150 A, 10.5 V, and 1.7 mm s^{-1} welding speed.

tration gradients are observed only in small areas near the edges of the weld pool, while the concentration of sulfur is fairly uniform in most of the central region of the weld pool surface and in the bulk of the weld pool. This observation is contrary to the previous [5] suggestion that a spatial gradient of sulfur concentration exists on the weld pool surface when two plates having different sulfur contents are welded.

What causes the absence of any significant sulfur concentration gradient in the weld pool when welding two plates with very different sulfur concentrations? To understand the transport of sulfur within the weld pool, the roles of convection and conduction in the overall transport of sulfur in the weld pool is examined from the value of the Peclet number for mass transfer, Pe_m , which is defined as:

$$Pe_m = \frac{uL}{D}, \quad (17)$$

where D is the mass diffusivity of sulfur. The value of mass diffusivity of sulfur in the three alloys in the temperature range of interest is not available in the literature. An approximate value has been reported by Luo [28] as $1.0 \times 10^{-8} \text{ m}^2 \text{ s}^{-1}$. Assuming a typical value of u for case 1 of Table 6 as 0.235 m s^{-1} and the value of L as 0.0024 m , the Pe_m is calculated to be 5.6×10^4 . This large

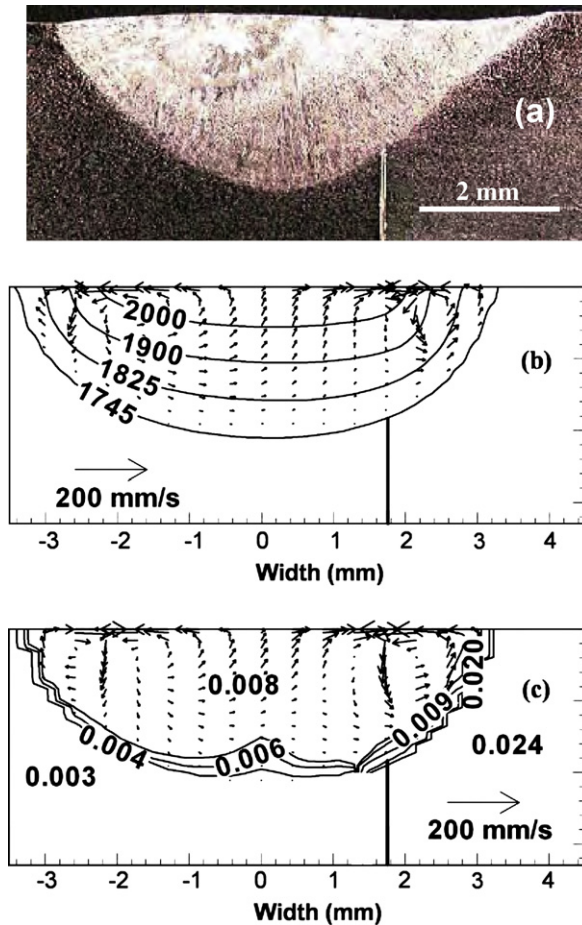


Fig. 9. Results for weld 3 in Table 6. (a) Experimental weld pool geometry. The vertical line shows the joint of the two plates. (b) Calculated temperature and velocity fields in the weld pool. The contours represent the temperatures in degree Kelvin and the vectors represent the liquid velocity. (c) The contours represent calculated sulfur concentrations in wt.%. The sulfur concentration on the top surface and the bulk of the weld pool was about 0.008 wt.%. Welding conditions: 150 A, 10.5 V, and 1.7 mm s^{-1} welding speed.

value indicates that convection is the primary mode of solute transport in the weld pool. For weld 1 in Table 6, the length of the weld pool is approximately 7 mm and the welding speed is 1.7 mm s^{-1} . Therefore, the duration for which any location along the welding direction on the top surface remains liquid is approximately equal to 4 s. Considering an average fluid velocity on the top surface as 100 mm s^{-1} , and two recirculating loops, it would take only about 0.035 s to travel a distance equal to half the length. Hence the surface can be replenished more than 100 times in the period a particular location remains liquid. The strong recirculating flow ensures rapid mixing of all sulfur in the weld pool and the absence of any significant concentration gradient except near the solid/liquid interface. Furthermore, the aforementioned discussion illustrates that it is necessary to consider convective mass transport in order to accurately predict the sulfur distribution in the weld pool.

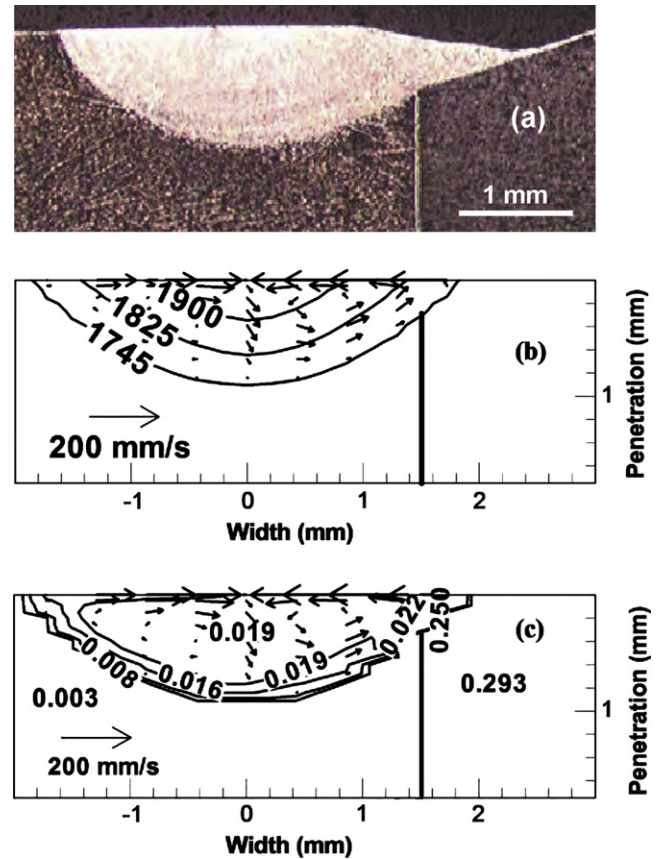


Fig. 10. Results for weld 10 in Table 6. (a) Experimental weld pool geometry. The vertical line shows the joint of the two plates. (b) Calculated temperature and velocity fields in the weld pool. The contours represent the temperatures in degree Kelvin and the vectors represent the liquid velocity. (c) The contours represent calculated sulfur concentrations in wt.%. The sulfur concentration on the top surface and the bulk of the weld pool was about 0.019 wt.%. Welding conditions: 100 A, 10.2 V, and 3.4 mm s^{-1} welding speed.

Fig. 8b shows the computed temperature and velocity fields for the welding of two plates with 0.293% and 0.003% sulfur. The sulfur concentration in most regions of the weld pool resulting from the mixing of the sulfur from the two plates is 0.026% as observed from Fig. 8c. For this concentration of sulfur, the temperature coefficient of surface tension is positive in a large range of temperature as observed from Fig. 1. As a result, the fluid motion at the surface of the weld pool is radially inward. Typical velocity in the weld pool is of the order of about 100 mm s^{-1} which is consistent with the values reported in the literature. The downward motion of the hot fluid in the middle of the weld pool results in a relatively deep weld pool. The location of the weld pool is shifted from the original interface of the two plates because of the arc asymmetry discussed previously. The temperature field shows slight asymmetry due to the complex mixing of the sulfur in the weld pool demonstrating the need to model this system in three dimensions. The peak temperature is slightly higher than 2000 K which is well within the temperature range reported in the literature. A similar

behavior of mixing of sulfur from the two plates with different sulfur concentrations, radially inward velocity field and the movement of the weld pool from the original interface of the two plates are shown in Figs. 9 and 10. Since the important features of these figures are the same as those of Fig. 8, these are not discussed separately.

The effects of the magnitude of difference in sulfur content between the two plates for welds made with identical parameters can be seen by comparison of Figs. 8 and 9. The CLS and extent of undercut are decreased for weld 3 (with a smaller difference in sulfur content, Fig. 9) relative to weld 1 (Fig. 8). The effects of changes in heat input for welds made between the same set of plates can be seen by comparison of Figs. 8 and 10. The CLS and depth of penetration for weld 10 (with lower heat input, Fig. 10) are less than for weld 1 (Fig. 8).

For each weld, the sulfur and phosphorus concentrations were measured using EPMA at the weld pool top surface along the y -direction, i.e. along the width as well as along a vertical line in the middle of the fusion zone, as shown by the dotted lines in Fig. 11. Fig. 12a–c shows the sulfur distribution on the top surface for the welds identified in Table 6 as welds 1–3, respectively. Fig. 13a–c shows the sulfur distribution along the weld pool depth for the same cases. The concentration profiles in Figs. 12 and 13 show that there is no significant concentration gradient of sulfur on the weld pool surface except very close to the fusion boundary near the weld pool edges. The computed sulfur concentrations were in reasonable agreement with the corresponding values in all cases. The measurements and the computed sulfur concentrations preclude any possibility of a concentration gradient induced net fluid flow at the liquid metal toward the low sulfur side. Therefore, the surface concentration gradient does not play a major role in shifting of the weld bead toward the low sulfur plate. The flaring of the arc towards the low sulfur side seems to be an important factor governing the fusion zone shift. Determination of the concentration profiles of phosphorous for weld 3 showed that no significant amount of phosphorous was lost from the weld pool due to welding.

Fig. 14 shows the variation of weld pool penetration with energy input per unit length for the 12 cases listed in Table 6. It can be seen that for a given SS pair the weld

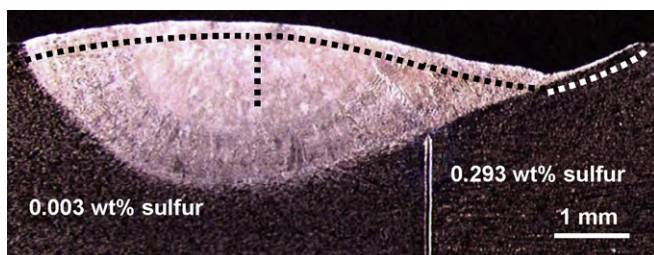


Fig. 11. The EPMA measurements of sulfur and phosphorus concentrations were measured along the dotted lines.

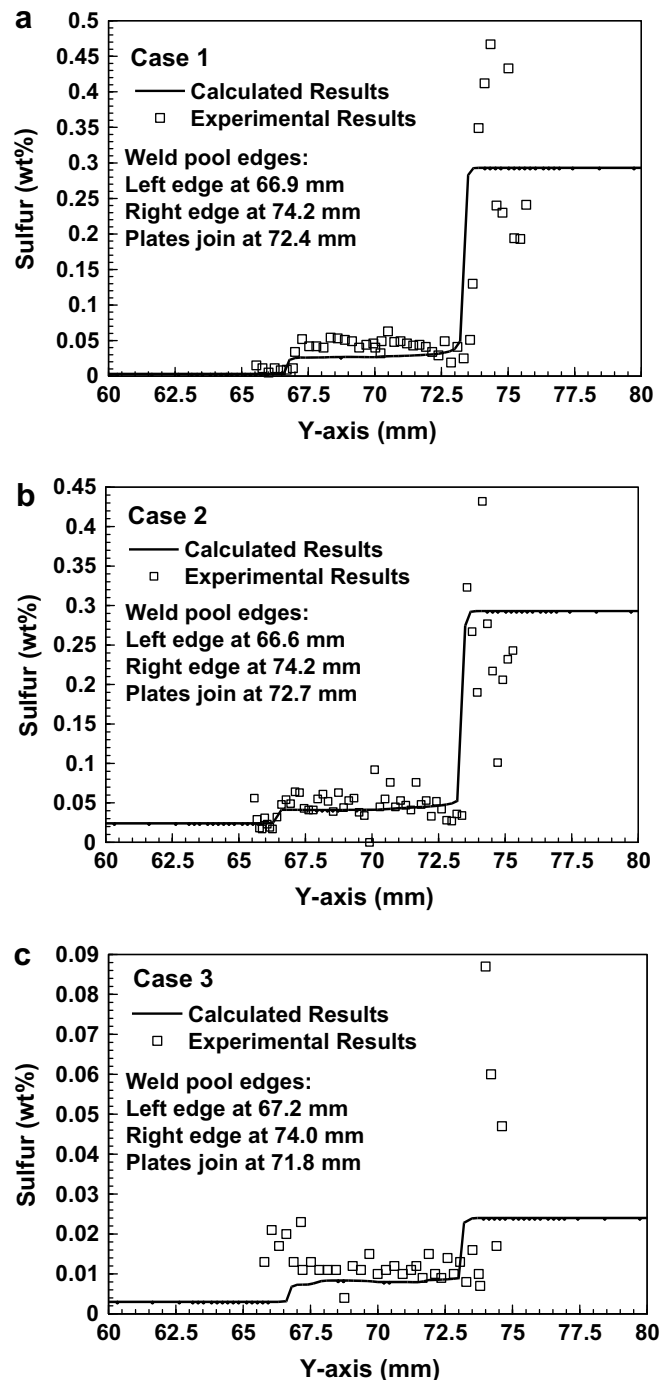


Fig. 12. Experimental and calculated sulfur concentrations along the horizontal dotted line shown in Fig. 11 for (a) case 1, (b) case 2, and (c) case 3 of Table 6. The symbols represent the experimental data and the solid line represents the calculated results.

pool penetration was higher for higher energy input, which is anticipated. The data show some scatter mainly resulting from the variations in the arc asymmetry in different cases. It is fair to say from Figs. 8–10, and from simulation results not shown here, that the calculated weld pool geometry was in fair agreement with the corresponding experimental results. The agreement shows the validity of the calculation procedure in predicting the

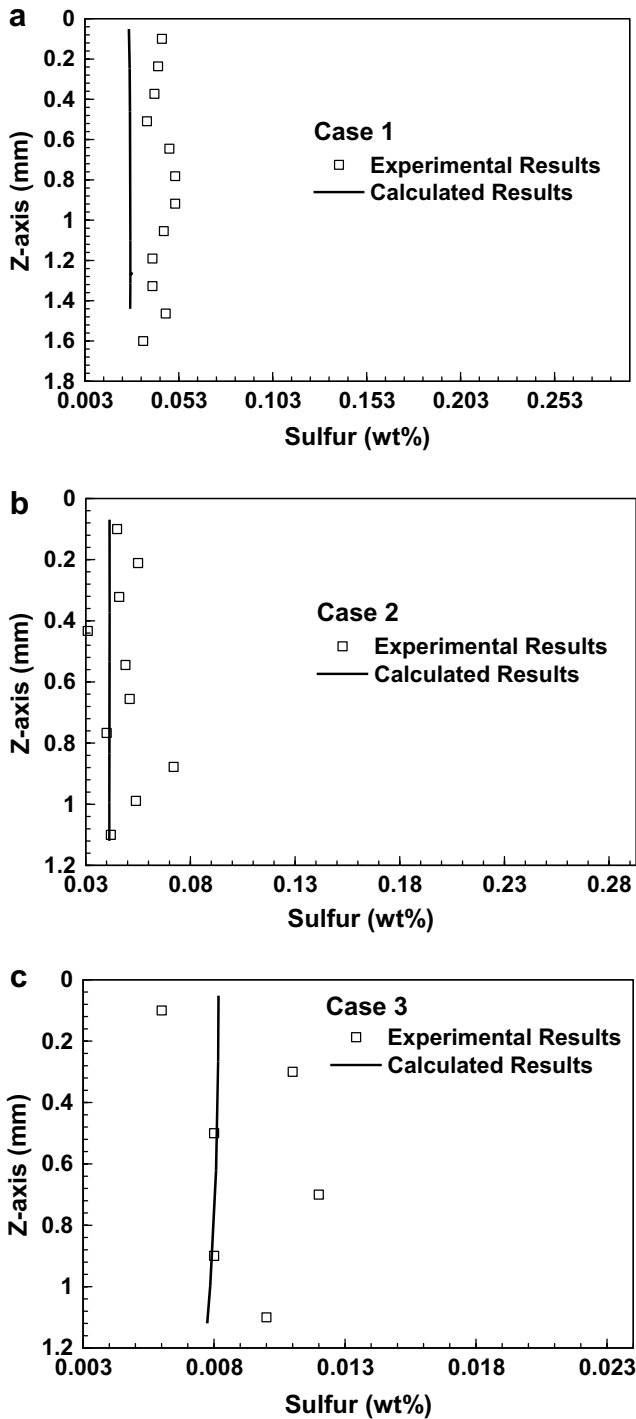


Fig. 13. Experimental and calculated sulfur concentrations along the vertical dotted line shown in Fig. 11 for (a) weld 1, (b) weld 2, and (c) weld 3 of Table 6. The symbols represent the experimental data and the solid line represents the calculated results.

weld pool geometry during welding of SSs with different sulfur contents. Furthermore, the results of the work indicate that calculations must incorporate the effects of both the sulfur distribution in the weld pool and the arc asymmetry to correctly understand the joining of plates with different sulfur contents.

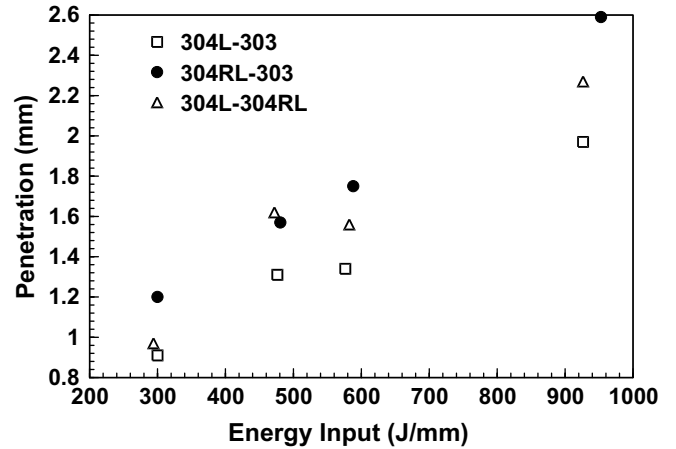


Fig. 14. Variation of weld pool penetration with energy input per unit length for 12 cases given in Table 6. The three stainless steel combinations welded together are: 304L welded to 303, 304RL welded to 303, and 304L welded to 304RL. The sulfur contents of the three stainless steels used are: 304L (0.003 wt%), 304RL (0.024 wt%) and 303 (0.293 wt%).

5. Conclusions

When two SS plates with different concentrations of sulfur were GTA welded, the fusion zone shifted significantly towards the low sulfur side, often resulting in a missed joint weld where the maximum penetration was well inside the low sulfur component and not at the joint. Two contributing factors for the formation of the weld pool, i.e. the flaring of the arc towards the low sulfur side and the role of sulfur in shaping the weld pool geometry were investigated. Both experimental measurements and the modeling results indicated that sulfur from both the plates mixed rapidly and there was no significant gradient of sulfur concentration in the weld pool except very close to the edges along the fusion boundary. Although the sulfur concentration of the weld pool affected weld geometry, flaring of the arc towards the low sulfur side was found to be an important factor governing the shifting of the weld pool and the missed weld joint. The CLS, i.e. the distance by which the maximum weld pool penetration was shifted from the plate joint, was found to be dependent on the difference in the sulfur concentrations of the two plates and the heat input. No significant bead shift was observed when two SS plates had the same concentration of sulfur. Numerical modeling of heat transfer, fluid flow and sulfur transfer was successfully accomplished by assuming that the arc was shifted by a distance equal to the experimentally measured value of CLS in each case. For the conditions of welding, convection was the main mechanism of heat transfer in the weld pool. High concentrations of sulfur in the weld pool increased its depth to width ratio. The calculated weld pool geometry and the sulfur concentration in the weld pool were in good agreement with the corresponding experimental results for the welding of plates with different sulfur contents, indicating the validity of the modeling approach.

Acknowledgments

The authors express gratitude to Mr. William Stellwag for conducting welding experiments and to Mr. Brandon Ribic and Mr. John Bernal for performing optical metallography.

Appendix A. Calculation of possible sulfur loss from the top surface

The loss of sulfur from the top surface involves two steps: (i) transfer of sulfur from the bulk to the weld pool surface and (ii) vaporization of sulfur from the surface. The flux of sulfur from the bulk to the surface, J_S , is given as [29]:

$$J_S = -D \frac{dC}{dz} = D \frac{C_{\text{sur}} - C_{\text{bulk}}}{\Delta z}, \quad (\text{A1})$$

where D is the diffusion coefficient of sulfur in molten steel, C_{sur} is the concentration of sulfur at the top surface, C_{bulk} is the concentration of sulfur in the bulk and Δz is the distance along the z -direction. The evaporation flux of sulfur vapor, J_B , is given as [30]:

$$J_B = k_{M,e}(C_{\text{sur}} - C_{\text{amb}}), \quad (\text{A2})$$

where $k_{M,e}$ is the evaporation mass transfer coefficient and C_{amb} is the concentration of sulfur in the vapor phase. Assuming mass conservation at the top surface, J_S becomes equal to J_B . Combining Eqs. (A1) and (A2) and assuming $C_{\text{amb}} = 0$ gives the mass loss boundary condition at the top surface as:

$$C_{\text{sur}}(i+1) = C_{\text{bulk}}(i) - \frac{k_{M,e} \times C_{\text{sur}}(i)}{D/\Delta z}, \quad (\text{A3})$$

where i denotes the current iteration and $i+1$ denotes the next iteration and Δz is the distance along the z -direction. The value of $k_{M,e}$ was obtained from the study of Ohno and Ishida [31]. Ohno and Ishida calculated the value of k_i for four alloys and, based on their measurements [31], an average value of $7.2 \times 10^{-6} \text{ m s}^{-1}$ has been used for $k_{M,e}$ in the present study. Owing to the low value of $k_{M,e}$, the sulfur loss from the top surface was not significant for the conditions of this study.

References

- [1] Pitscheneder W, DebRoy T, Mundra K, Ebner R. *Weld J* 1996;75:71s.
- [2] Sahoo P, DebRoy T, McNallan MJ. *Metall Trans B* 1988;19:483.
- [3] Heiple CR, Roper JR. *Weld J* 1982;61:97s.
- [4] Heiple CR, Roper JR, Stagner RT, Alden JJ. *Weld J* 1983;62:72s.
- [5] Heiple CR, Burgardt P, Roper JR, Long JL. In: Proceedings of the international conference on the effects of residual, trace and micro-alloying elements on weldability and weld properties. Cambridge: TWI; 1984. p. 36.
- [6] Pierce SW, Burgardt P, Olson DL. *Weld J* 1999;78:45s.
- [7] Keene BJ, Mills KC, Robinson JL, Rodwell MH. In: Proceedings of the international conference on the effects of residual, trace and micro-alloying elements on weldability and weld properties. Cambridge: TWI; 1984. p. 45.
- [8] Leinonen J, Karjalainen LP. In: Proceedings of the international conference on the effects of residual, trace and micro-alloying elements on weldability and weld properties. Cambridge: TWI; 1984. p. 4.
- [9] Autio J, Makio J, Makela K, Minni E, Kettunen P. In: Proceedings of the international conference on the effects of residual, trace and micro-alloying elements on weldability and weld properties. Cambridge: TWI; 1984. p. 18.
- [10] Rollin AF, Bentley MJ. In: Proceedings of the international conference on the effects of residual, trace and micro-alloying elements on weldability and weld properties. Cambridge: TWI; 1984. p. 9.
- [11] Rodgers KJ. In: Proceedings of the international conference on the effects of residual, trace and micro-alloying elements on weldability and weld properties. Cambridge: TWI; 1984. p. 2.
- [12] Tinkler MJ, Grant I, Mizuno G, Gluck C. In: Proceedings of the international conference on the effects of residual, trace and micro-alloying elements on weldability and weld properties. Cambridge: TWI; 1984. p. 29.
- [13] Kolman DG. Assessment of the corrosion, stress corrosion cracking and embrittlement susceptibility of 30313 storage containers. <<http://public.lanl.gov/MCEL/PDF-Publications/CorrSCC3013.pdf>>.
- [14] Cannell GR, Daugherty WL, Stokes MW. Closure welding of plutonium bearing storage containers. <<http://sti.srs.gov/fulltext/ms2002053/ms2002053.pdf>>.
- [15] US Department of Energy Report DOE-STD-3013-96. Criteria for preparing and packaging plutonium metals and oxides for long-term storage. <<http://www.eh.doe.gov/techstds/standard/std3013/s963013.pdf>>.
- [16] Zhang W, Roy GG, Elmer J, DebRoy T. *J Appl Phys* 2003;93:3022.
- [17] Mundra K, DebRoy T, Kelkar K. *Numer Heat Transfer A* 1996;29:115.
- [18] Brent AD, Voller VR, Reid KJ. *Numer Heat Transfer* 1988;13:297.
- [19] Kumar A, DebRoy T. *J Appl Phys* 2003;94:1267.
- [20] De A, DebRoy T. *J Phys D: Appl Phys* 2004;37:140.
- [21] De A, DebRoy T. *J Appl Phys* 2004;95(9):5230.
- [22] McNallan MJ, DebRoy T. *Metall Trans B* 1991;22B:557.
- [23] Brandes EA, Brook GB, editors. *Smithells metals reference book*. Oxford: Butterworth-Heinemann; 1992.
- [24] Bennett WS, Mills GS. *Weld J* 1974;53:548s.
- [25] Dunn GJ, Eagar TW. *Weld Res Council Bull* 1990;357:22.
- [26] Abbaoui M, Cheminat B, Andanson PJ. *J Phys D: Appl Phys* 1985;18:L159.
- [27] Wei PS, Wen CW. *Metall Mater Trans B* 2002;33B:765.
- [28] Luo H. *Scand J Metall* 2001;30:212.
- [29] Bird RB, Stewart WE, Lightfoot EN. *Transport phenomena*. New York: John Wiley; 1960.
- [30] Geiger GH, Poirier DR. *Transport phenomena in metallurgy*. Reading, MA: Addison-Wesley; 1973.
- [31] Ohno R, Ishida T. *J Iron Steel Inst* 1968;206:904.